MOLEKUL
eISSN: 2503-0310

Articles
https://doi.org/10.20884/1.jm.2023.18.3.6630

Development and Characterization of Edible Films Based on Gelatin/Chitosan Composites Incorporated with Zinc Oxide Nanoparticles for Food Protection

Asrul Bahar[1], Samik Samik[2], Maria Monica Sianita[2], Nita Kusumawati[2]*, Ianatul Khafidlah[2], Supari Muslim[3], AR. Sella Auliya[4]

[1] Departement of Family Welfare Education, Universitas Negeri Surabaya, Surabaya, 60231, Indonesia
[2]Departement of Chemistry, Universitas Negeri Surabaya, Surabaya, 60231, Indonesia
[3]Departement of Electrical Engineering, Universitas Negeri Surabaya, Surabaya, 60231, Indonesia
[4]Departement of Chemistry, Airlangga University, Mulyorejo, Surabaya, 60115, Indonesia

*Corresponding author email: nitakusumawati@unesa.ac.id

Received September 02, 2022; **Accepted** June 20, 2023; **Available online** November 20, 2023

ABSTRACT. Globally produced food products spoil before they reach consumers. Therefore, active biodegradable packaging is needed to overcome cases of global environmental pollution due to plastic waste, and it is hoped that it can keep food products from reaching the sales stage. Gelatin (G), is one of the potential edible film raw materials. However, its weak water barrier and mechanical properties have limited its wide application. The combination of zinc oxide nanoparticles (ZnONP) and chitosan nanofiber (CHNF) is anticipated to enhance the G film's mechanical and barrier characteristics as well as provide antioxidant and antibacterial capabilities. Characterization results using FTIR, SEM, and DSC showed good compatibility between the G, CHNF, and ZnONP matrixes. The results of the packaging tests revealed that composite films based on gelatin, CHNF, and ZnONP showed potential as a functional material for food packaging.

Keywords: CHNF, Edible, Gelatin, Packaging, ZnONP

INTRODUCTION

Food and Agriculture Organization (FAO) research indicates that 14% of food products produced globally are harmed before being sold (Susmitha et al., 2021). Short shelf life due to the susceptibility of dairy products to microbial contamination even before consumption is one of the main problems that trigger waste. The delicious taste and content of several intrinsic nutrients make cheese one of everyday life's most consumed food products. However, during storage and production of the cheese, pathogenic Staphylococcus aureus and Listeria monocytogenes might proliferate (Lin et al., 2019). As a solution, packaging that can enhance cheese's shelf life is used. Most food packaging comes from synthetic plastics, which do not biodegrade in nature. The intensive production, application, disposal, and stockpiling of this packaging significantly negatively impacts society and the environment (Liu et al., 2020). Thus, it's essential to create biopolymer packaging that is affordable, biodegradable, renewable, accessible in nature, and environmentally benign (Lin et al., 2019).

Gelatin (G) is a potential biopolymer for the creation of biodegradable packaging due to its availability, biodegradability, excellent oxygen barrier capability, low gelling and melting temperatures, and ability to act as a functional agent carrier (Amjadi et al., 2019; Bahar et al., 2020; Kusumawati et al., 2019; Bahar et al., 2018; Bahar et al., 2019). However, due to gelatin's poor water barrier characteristics and low mechanical strength, its usage in food packaging has been restricted (Quero et al., 2018). This issue has been resolved by modifying a number of processes, such as adding nanoparticles to increase mechanical resistance, employing a variety of chemicals to improve barrier qualities, and using the antioxidant and antibacterial properties of the biopolymers (Amjadi et al., 2019).

Chitosan (CH) biopolymer, like gelatin, can be employed in the creation of food packaging because of its biocompatibility and low toxicity (Davoodi et al., 2020). Due to their high surface area to volume ratio and excellent mechanical strength when combined with other polymers, chitosan nanofibers (CHNF) are the most prominent of their physical forms. In order to strengthen the mechanical resistance of gelatin packaging while decreasing WVP (Water Vapor Permeability), which is the capacity of an edible film to tolerate the rate of water vapor passing through it, chitosan nanofibers (CHNF) may be added.

The G-CHNF film's antioxidant and antibacterial activity is anticipated to be enhanced with the inclusion

of zinc oxide nanoparticles, generating an active package that can offer the best defense against the propagation of the virus. Yadav et al. (2021) reported zinc oxide nanoparticles' (ZnONPs) all-around antibacterial efficacy (Yadav et al., 2021). These nanoparticles also possess improved photocatalytic properties, a higher surface-to-volume ratio, surface reactivity, and antioxidant activity in addition to being more stable and non-toxic (Kamdem et al., 2019). The United States has given its approval for ZnONP to be used in pharmaceuticals, cosmetics, and food packaging. This method requires the development and characterization of edible gelatin/chitosan film composites containing zinc oxide nanoparticles for food protection.

EXPERIMENTAL SECTION

Materials

The materials and their specifications used in this study were gelatin from commercial cowhide (gel strength 225 g bloom, type-B), CH_3COOH 2%, CHNF, and ZnONP. ZnONPs powder (95% of the particles had a mean diameter of 20–30 nm) was purchased from Peter ShiZengou Farm-Reaching Biochemical Co. (Jiangsu, China). For the antimicrobial test, Mueller-Hinton agar (Sigma-Aldrich, Singapore) nutrient broth media (Millipore, Singapore) *Staphylococcus aureus* (ATCC®12600TM, IBRC), *Escherichia coli* (ATCC®8739TM, IBRC), and *Pseudomonas aeruginosa* (ATCC®10145TM, IBRC).

Preparation of Composite Films

The casting knife technique was used to create films with different thicknesses (0.8-1.2 mm) of G, G.CHNF, G.ZnONPs, and G.CHNF.ZnONPs. The 4% (w/v) gelatin solution was stirred using a hot plate magnetic stirrer (45 ºC; 30 minutes). In a different place, the CHNF solution was prepared with a composition of 10% by weight of dry gelatin, dissolved in 2% acetic acid, and stirred (50 °C; 120 minutes), while the ZnONP solution was prepared with a composition of 5% by weight of dry gelatin, dissolved in 2% acetate acid and stirred (100; 360 min). Glycerol plasticizer prepared with a composition of 25% by weight of dry gelatin, dispersed in a 4% gelatin solution supplemented with previously prepared CHNF, ZnONP, and CHNF-ZnONP (1:1) solutions, then stirred (25 °C; 60 min). To ensure that the film solution was free of air bubbles, the films were degassed by ultrasound at 30 ºC for 30 minutes. The film solution was then applied to a 14 × 14 cm acrylic plate and allowed to air dry for 72 hours at room temperature. The dried films were kept in a desiccator for 72 hours at 25 °C and 50% relative humidity before testing (Amjadi et al., 2019).

Film Characterization

The structural interactions of the films were evaluated using Perkin Elmer Spectrum Two FTIR spectroscopy (China). FEI Inspect-S50 SEM (Canada) was used to assess the films' morphology, surface, and cross-section. In particular, cross-sectional films were fabricated using Mikrotomy Microm, HM315 (Germany). The Linseis STA PT 1600 DSC (Germany) assessed the film's thermal stability between 20 and 300 °C. The mechanical parameters of the film were tested using an autograph, AG-10TE (Japan). Water absorption was evaluated based on the Amjadi (2019) method (Amjadi et al., 2019). The film's water vapor permeability was assessed using the ASTM E96-05 standard procedure (ASTM, 2005). Transparency and light transmittance, as well as the film color parameters (CieLab coordinates), such as brightness (L*), reddish/greenish (a*), and yellowish/bluish (b*), were measured with a Shimadzu UV-2401-PC spectrophotometer (Japan). The antibacterial effectiveness of the movie was evaluated using the agar diffusion method.

RESULTS AND DISCUSSION

Fourier Transform Infra-Red

The Fourier Transform Infrared method was used to assess the structural interactions of the films. All composite films in **Figure 1** showed similar specific peaks: 1) the amide-A band at 3283.99 - 3289.17 cm^{-1} which also indicates a secondary amine group; and 2) the amide-B band at 2936.40 - 2937.38 cm^{-1}. Amide-I, amide-II, and amide-III have distinct peaks at 1629.54 - 1633.88 cm^{-1}; 1538.64 - 1547.98 cm^{-1}; 1238.38 - 1239.40 cm^{-1}, respectively, these peaks are likewise present in all films. The creation of cross-links between the peptide chains is indicated by the amide-I and amide-II bands. Amidate-III band, meanwhile, demonstrates the protein's capacity to preserve the triple helix complex (Cai et al., 2019).

The addition of CHNF causes a change in wavenumber specifically in the amide-A, amide-I, amide-II, and amide-III bands as a result of the formation of intramolecular hydrogen bonds in chitin during electrospinning. The creation of hydrogen bonds between the N-H groups of gelatin and ZnONPs results in a shift that is also brought on by the presence of ZnONPs. The incorporation of CHNF and ZnONPs also causes a shift in the G.CHNF.ZnONPs film due to the interaction between -OH, -COOH, and $-NH_2$ groups combine with -COO, -OH, and $-NH_2$ groups in CHNF and Zn^{2+} in ZnONPs (Ge, et al., 2018).

All nanocomposite films also showed interactions with glycerol, which were observed at 1033.92 cm^{-1} (G); 1033.29 cm^{-1} (G.CHNF); 1032.28 cm^{-1} (G.ZnONPs); and 1032.40 cm^{-1} (G.CHNF.ZnONPs). In particular, the amide-A band saw a wavenumber shift when the G.CHNF.ZnONPs nanocomposite film's thickness changed (**Figure 2**). The amide-A band was measured at 3287.26 cm-1 at a thickness of 1.0 mm, and at 3286.50 cm-1 at a thickness of 1.4 mm. This change is a result of the molecules of chitin and gelatin forming hydrogen bonds with one another (Ge et al., 2018).

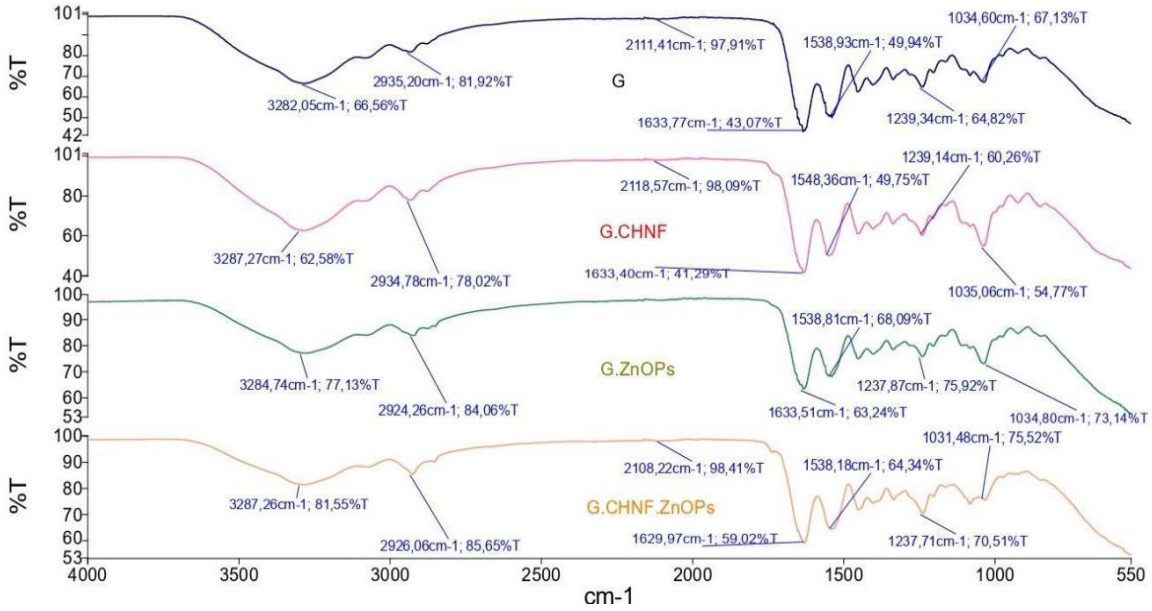

Figure 1. Fourier transform infrared (FTIR) spectrum of the compounds G, G.CHNF, G.ZnONPs, and G.CHNF ZnONPs

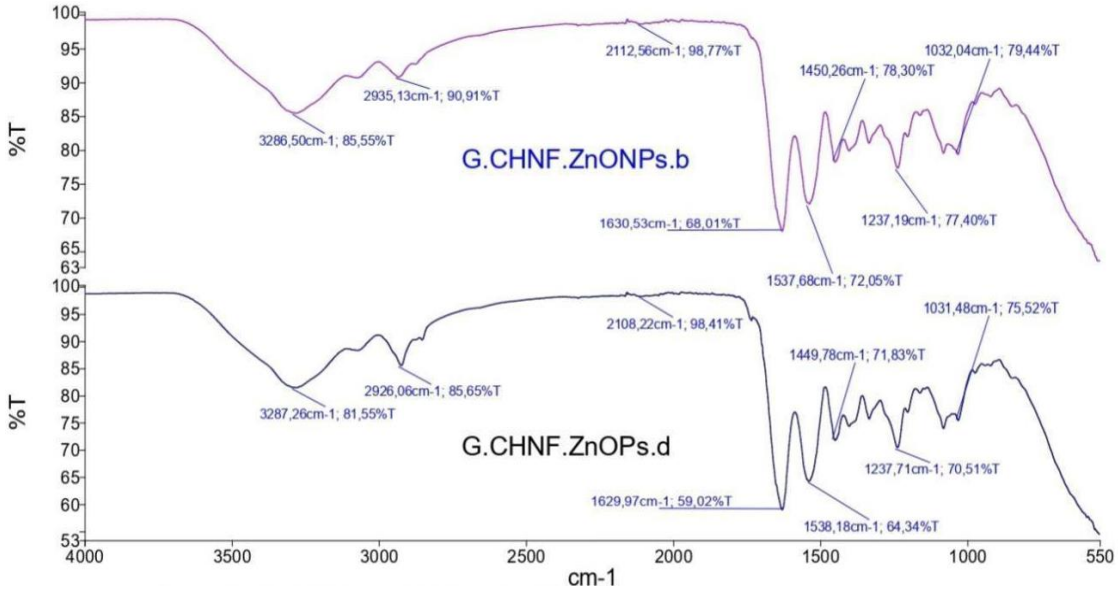

Figure 2. The infrared spectrum of G.CHNF.ZnONPs film with various casting thicknesses: 1.0 mm (**b**) and 1.4 mm (**d**)

Scanning Electron Microscopy

The Scanning Microscopy (SEM) outcomess of G, G.CHNF, GZnOPs, and G.CHNF.ZnONP are shown in **Figure 3.** According to the SEM results, the G film's surface seems to be uneven and to have pores and cracks in it. In addition, the filamentous structure of CHNF, which was introduced, caused substantial changes in the interconnected pore microstructure. Demonstrate how the porous structure makes it easier for ZnONP to connect to the film matrix, increasing density and compactness while decreasing porosity, cracking, and improving mechanical and thermal stability while also boosting water barrier qualities.

Film thickness was also detected to affect the morphology of the G.CHNF.ZnONPs nanocomposite films (**Figure 4**). An increase in the cast thickness causes an increase in the availability of solids thereby increasing the density and compactness of the film matrix, (Ansari et al., 2018). In the work by Li et al. (2021), it was found that the surface roughness of polyethylene terephthalate (PET) optical films gradually decreased with an increase in coating thickness. **Figure 4** shows how the increased smoothness of the film's surface corresponds to the incremental cast thickness.

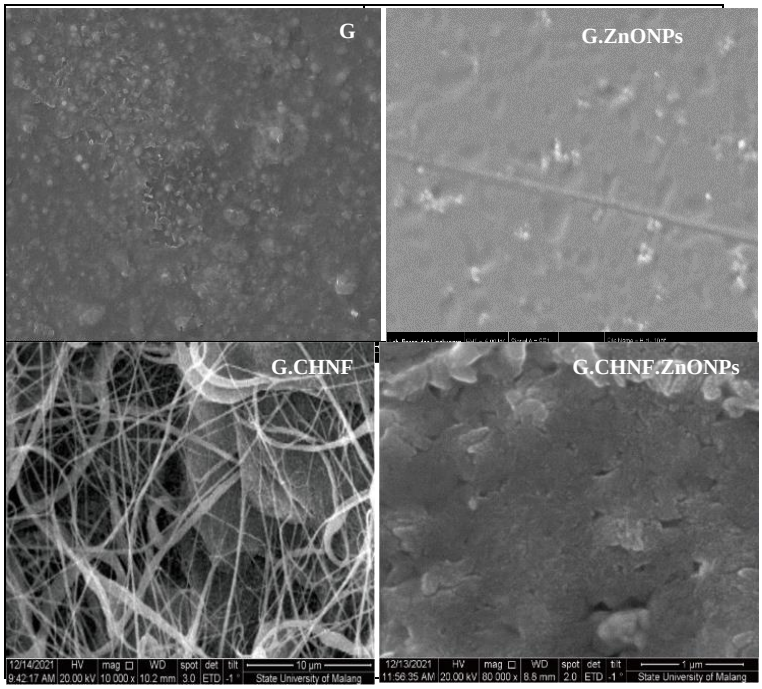

Figure 3. SEM images of film samples from the composition of G, G.ZnOPs, and G.CHNF (10,000x magnification) and G.CHNF.ZnOPs (80,000x magnification)

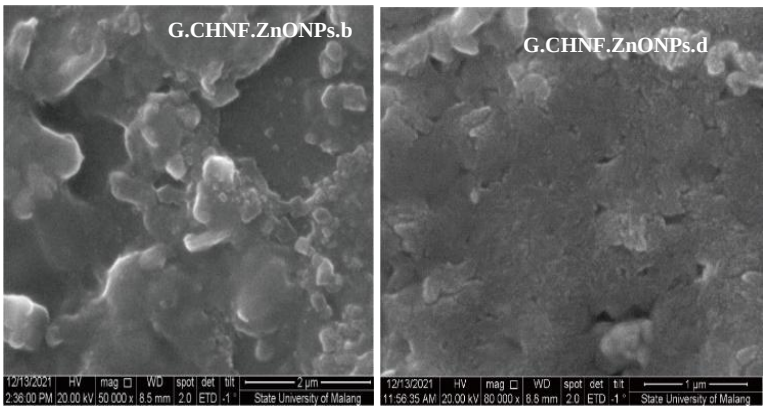

Figure 4. SEM images of the G.CHNF.ZnONPs film with variations in casting thicknesses: 1.0 mm (**b**) (50.000x magnification), and 1.4 mm (**d**) (80.000x magnification)

Differential Scanning Calorimetry

Results of Differential Scanning Calorimetry (DSC) tests on G, G.CHNF, GZnOPs, and G.CHNF.ZnONP are shown in **Figure 5**. DSC results show that the thermal analysis showed the appearance of two sharp endothermic peaks from the G film, namely at 124.05 °C which corresponded to the water vapor evaporation and the amino acid-rich region devitrification, and at 222.65 °C which corresponded to the imino-acid-rich region (proline and hydroxyproline) devitrification. The shift of the first (to 139.35 °C) and the second endothermic peak (to 213.45 °C) of the G.CHNF film were associated with increased evaporation of moisture content and decomposition of nanofiber, respectively (Ebrahimi, et al., 2019). A further shift was observed in the G.ZnONP film, where the first endothermic peak shifted to 174.55 °C and the second to 224.85 °C. Compared to the other three films, the most distant shift of the two endothermic peaks of the G.CHNF.ZnONP film, i.e. 185.55 for the first peak and 236.15 °C for the second showed a synergistic effect of CHNF, ZnONPs, and gelatin increasing the gelatin chain sequence and film crystallinity (Boura-Theodoridou et al., 2020).

Research by Zhang and Wang (2017), the heat resistance of the film was found to increase as one increases film thickness. The displacement of the first endothermic peak to 185.55 °C and the second peak to 236.15 °C in a G.CHNF.ZnONPs film with a 1.4 mm thickness in contrast to the 1.0 mm thickness is shown in **Figure 6**. The increase in thickness causes the formation of more crystal structures in the gelatin-CHNF nanocomposite film, one of which is due to CHNF nucleation (Wang et al., 2021).

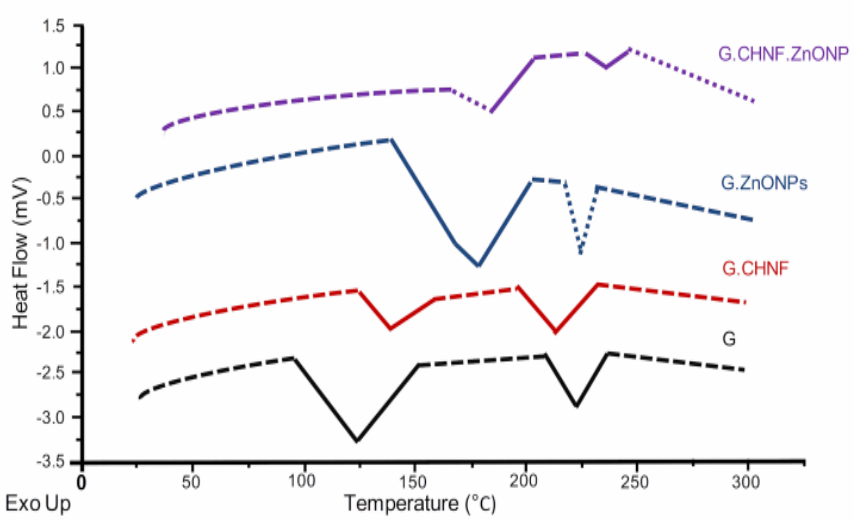

Figure 5. G, G. CHNF, G. ZnONPs, and G. CHNF.ZnONP DSC spectra

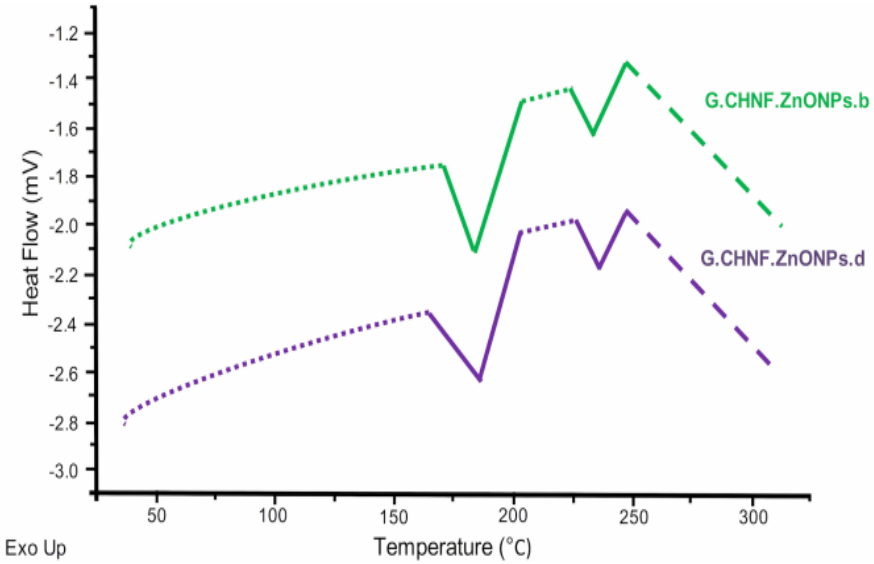

Figure 6. DSC spectrum G.CHNF.ZnONPs film with variations in casting thickness: 1.0 mm (b); and 1.4 mm (d)

Thickness and Mechanical Properties

Figure 7 shows an increase in film thickness after adding ZnONPs and a decrease in film thickness after adding CHNF. The existence of interconnected pores after the addition of CHNF allows the entry of ZnONPs into the polymer matrix, resulting in a thinner G.CHNF.ZnONP film than G.ZnONP. Film thickness was also found to increase with increasing casting thickness. The larger the volume of the casting solution, the more total solids in the cast area and the higher the thickness of the resulting film (Hari, et al., 2021). By examining the parameters of Young's modulus (YM), tensile strength (UTS), and elongation (ETB), which are shown in Figure 8, the mechanical characteristics of the film were assessed. **Figure 8** shows the higher UTS and YM of G.ZnONPs films than those of G films. The interaction in the matrix and mechanical characteristics of the film are improved by dispersion of ZnONP particles. On the other hand, the decrease in free volume between polymer chains due to ZnONP dispersion caused the polymer network to be less permeable, resulting in a decrease in ETB from 0.081 to 0.009% (Nandiwilastio et al., 2019). In line with this, the increase in crystallinity due to the formation of interconnected pore networks by CHNF created stronger interfacial interactions, thereby increasing UTS by 73.21% and YM by 80.33% of G.CHNF films. The presence of hydrogen bonds between chains further strengthens mechanical stability. The addition of CHNF also caused a decrease in ETB by 0.032% in the G.CHNF film. The increase in intermolecular and intramolecular interactions in the matrix after the addition of CHNF and ZnONP simultaneously resulted in lower flexibility and mobility of polymer segments compared to G.CHNF films (Al.-Tayyar et al., 2020).

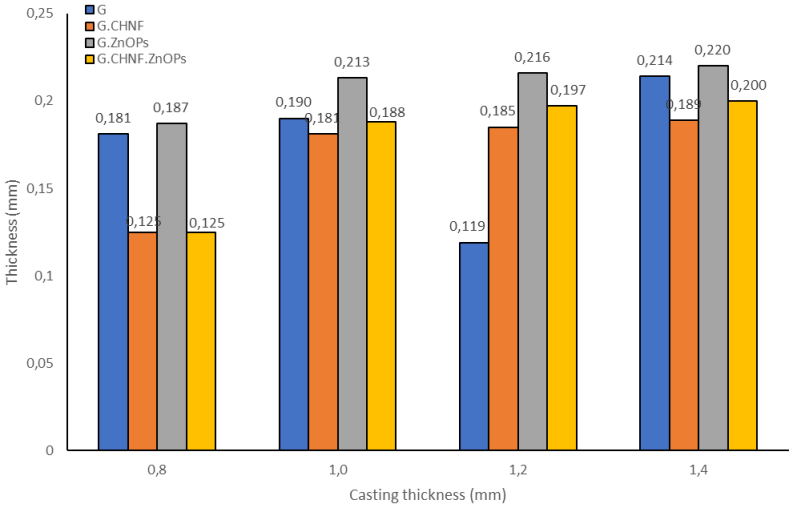

Data were expressed as a mean ±0.032 standard deviation

Figure 7. Film thickness with a variety of compositions and casting thickness

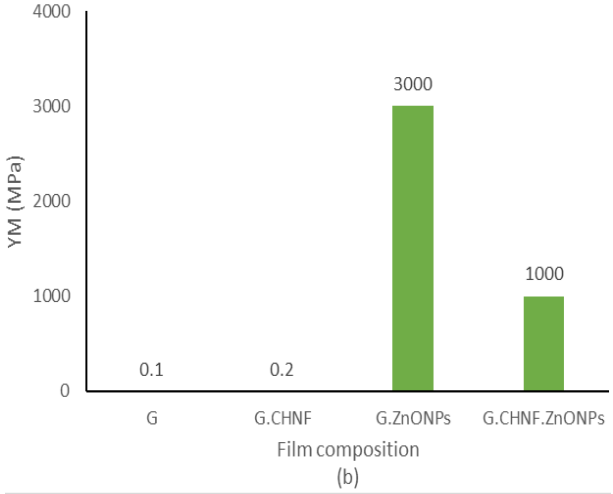

Data were expressed as mean ±19.26 standard deviation

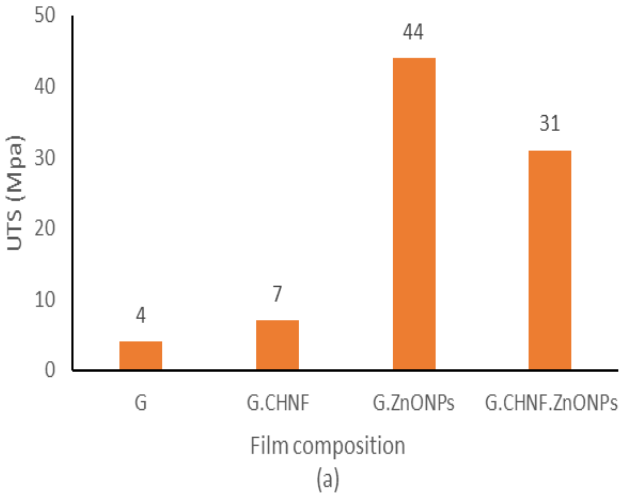

Data were expressed as mean ±1414.14 standard deviation

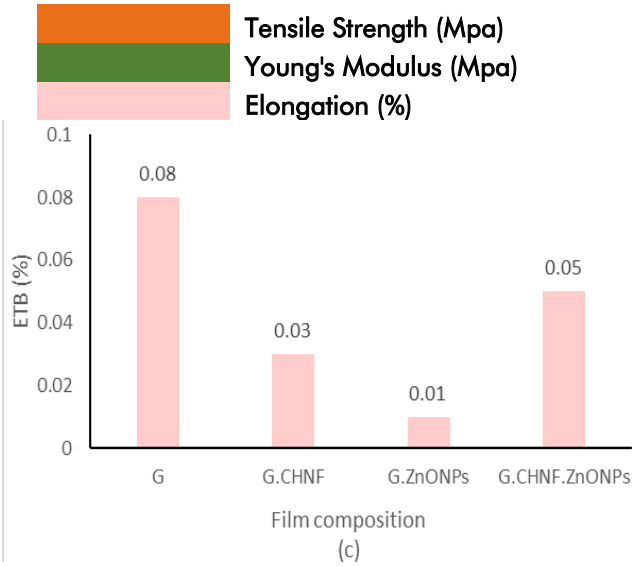

Data were expressed as mean ±0.03 standard deviation

Figure 8. Mechanical properties of film samples

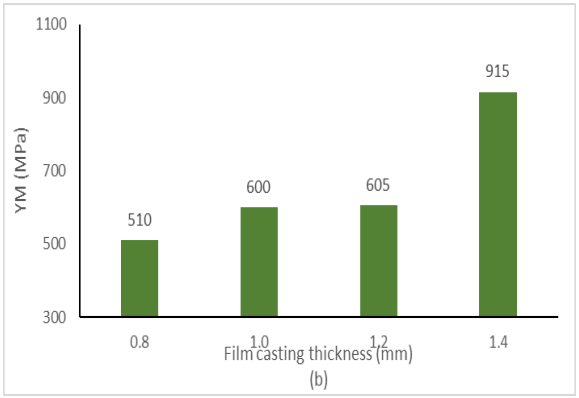

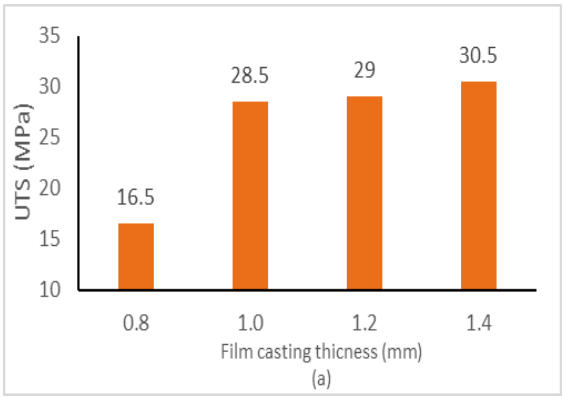

Data were expressed as mean ±6.47 standard deviation

Data were expressed as mean ±177.13 standard deviation

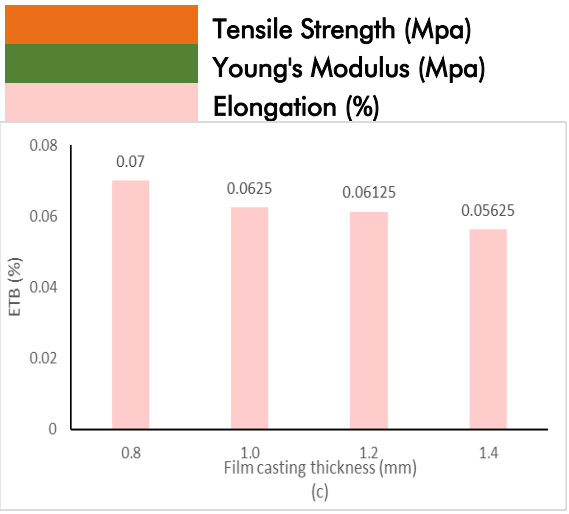

Data were expressed as mean ±0.0057 standard deviation

Figure 9. Film mechanical properties with variation in casting thickness

The thickness of the film also affects the mechanical characteristics of the nanocomposite film (Wafi, et al., 2020). The rise in UTS as film thickness increases is strongly proportional to molecular weight. The closer the distance between the molecules, the stronger the interactions. This condition creates an increase in UTS while decreasing ETB. The influence of thickness on G.CHNF.ZnONP mechanical characteristics film is shown in **Figure 9**.

Barrier Properties

Water absorption and water vapor permeability (WVP), two crucial characteristics, are frequently examined in studies of moisture transport. The moisture absorption and water permeability values after 96 hours of conditioning at 99% RH of the nanocomposite are shown in **Figure 10**. Despite the fact that G.CHNF and G films of the same thickness did not show any statistically significant difference ($p>0.05$), the percentage of water absorption in G films showed an upward trend. The percentage of water absorption in the G film decreased significantly ($p<0.05$) after ZnONP was added, peaking after CHNF and ZnONP were included. Increased cross-link formation due to The combination of both lowers the polymer chain's mobility.

The water vapor permeability (WVP) of the film showed the same pattern as the percentage of water absorption. In contrast to the effect of adding CHNF, hydrogen bonds formed between gelatin-ZnONP caused a decrease in free hydrophilicity, thereby reducing the WVP value of G.ZnONP films. The lowest WVP value was produced by G.CHNF.ZnONP film. These results indicate a more significant effect of adding ZnONP than CHNF on decreasing WVP (Soradech et al., 2017). The decrease in gelatin chain mobility resulted in a reduction in WVP characteristics while concurrently increasing the water barrier film.

Research by Rudakova et al. (2021) said that the more hydrophilic the film is, the thicker the TiO_2 layer. The fact that the hydrophilic nature of the film matrix largely determines WVP. The increase in thickness produces strain, which makes the matrix more brittle and prone to cracking. Under these conditions, water vapor flows faster through the resulting crack (Cai et al., 2020).

Transparency

Transparency is an important metric for determining the quality of packing materials and their capacity to filter UV radiation, which causes food product quality to deteriorate due to spoilage.

Figure 11b shows the transparency values for each film. Although not significant ($p>0.05$), G.CHNF film was found to have lower transparency than G film. The CHNF filament structure causes a decrease in light scattering on the CHNF-gelatin surface (Chen, et al., 2018). The dense and complex structure of ZnONP in the matrix further decreases light scattering and increases film opacity (Ngo, et al., 2018). The combination of CHNF and ZnONP made the G.CNF.The ZnONP film less clear than any other G film in this study. The G film, whether it had CHNF and ZnONP or not, or both, was also less clear than some common packaging materials, such as LDPE (which had a transparency value of 4.26) and strained polypropylene. (transparency value 1.57). Thickness also has the same effect on film transmission. Increasing the thickness will increase the number of layers formed, thereby reducing light transmission. The more layers of atoms that make up the film will trigger an intensification of the collision with the light particles, thus creating a significant barrier to transmission into the package (Roy & Rhim, 2021).

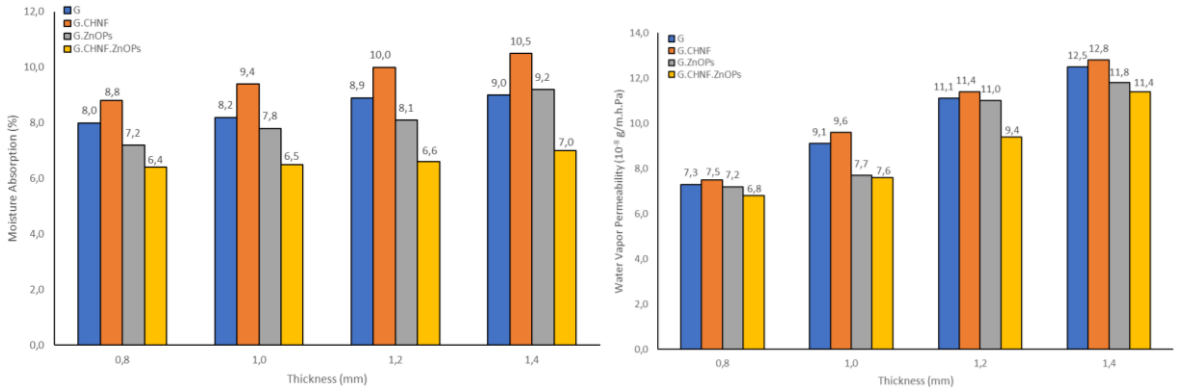

Data were expressed as a mean ±1.259 standard deviation standard deviation

Data were expressed as a mean ±2.087

Figure 10. Film's moisture absorption (a); and WVP (b) with variation of composition and casting thickness

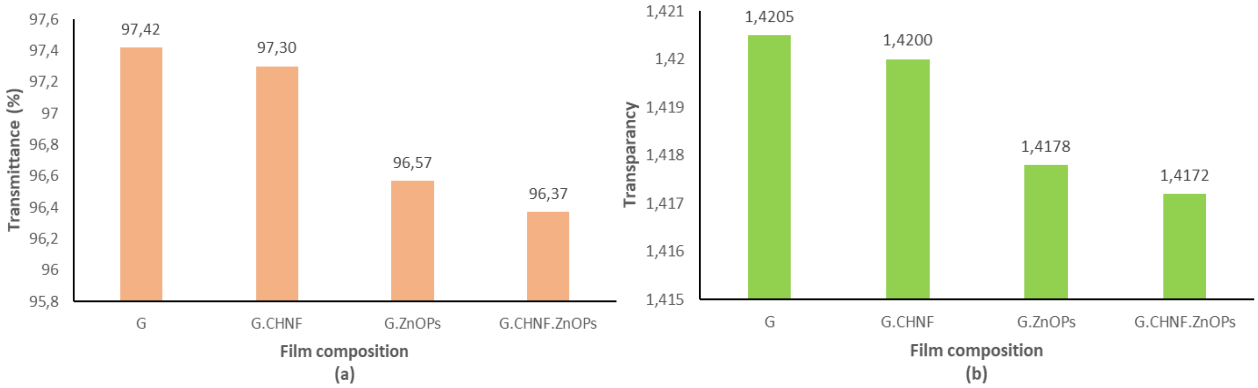

Data were expressed as mean ±0.523 standard deviation standard deviation

Data were expressed as mean ±0.002

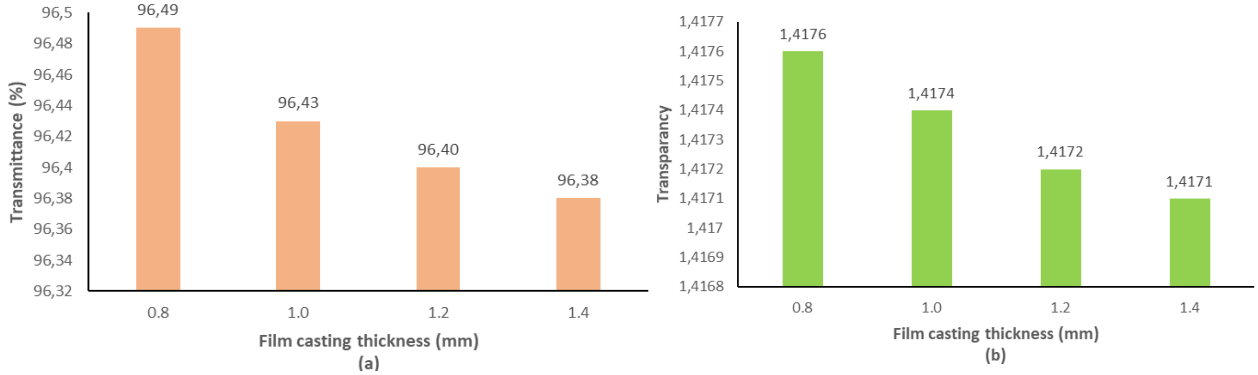

Data were expressed as mean ±0.048 standard deviation standard deviation

Data were expressed as mean ±0.0002

Figure 11. Film's transmittance (a) and transparency (b) with a variation of compositions (1) and casting thickness (2)

Color Properties

The color characteristic of the film has a significant impact on the look of the packaging as well as consumer acceptance of the product. The color properties parameters (L*, a*, b*, E, WI, and YI) like the film that is shown at **Table 1**. High collagen content causes the G film to have a clear color (Yusof & Zain, 2019). A decrease in the L* the value of G films was detected after CHNF addition. The CHNF filament structure reduces light scattering on the CHNF-gelatin surface, resulting in a decrease in transparency and L* value (Chen et al., 2018). Adding ZnONPs caused another noticeable drop ($p < 0.05$) in transparency and L* value, The light transmission is blocked by the thick and intricate structure of ZnONPs (Al-Tayyar et al., 2020).

G.CHNF film produced lower a* and higher b* values than G film, 0.26 and -0.34, respectively. This value indicates a greenish or reddish color tendency in the G.CHNF film. These results are related to the presence of 1-4 linked-2-amino-2-deoxy-D-glucopyranose in CHNF (Yusof & Zain, 2019). G.ZnONPs films showed similar results, with lower a* and much higher b* values than G films, 0.18 and -0.008, respectively. Thus, the G.ZnONPs films tend to have a bluish or yellowish color. The highest decrease in L* and a* values were obtained after the addition of CHNF and ZnONPs. The addition of both has an impact on increasing the b* value of the G.CHNF.ZnONPs film.

Table 2. displays how the color properties of G.CHNF.ZnONPs films change with the casting thickness. The L* and a* values of the film decrease as casting thickness increases. On the other hand, increasing casting thickness was found to increase the b* value. The tendency for reddish and dark hues to appear hinders visible light penetration through the film surface. Thus, the nutrition, color, and taste of packaged food products can be maintained (Kan et al., 2019).

Antibacterial Activity

The film's capacity to prevent and stop bacteria from spreading in food products that are wrapped was tested by an antibacterial activity analysis. The diameter of the film inhibitory zone for each bacteria is provided in **Tables 3-5**. G Film did not exhibit an inhibitory zone against the three test microorganisms. In contrast, G.CHNF films exhibited antibacterial activity as did G.ZnONP. However, G.ZnONPs films were much more effective in killing gram-positive bacteria than gram-negative bacteria. An outer membrane that blocks reactive oxygen species (ROS) makes gram-negative bacteria more resistant to ROS than gram-positive bacteria (Babaei-Ghazvini et al., 2021). With a different mechanism, the positively charged glucosamine amine group (NH_3^+) in CHNF will interact with the negatively charged outer membrane resulting in a pore that causes damage to intracellular components and causes bacterial cell death (Shankar et al., 2017).

G.CHNF.ZnONPs film showed the highest antibacterial activity. The combined effect of CHNF and ZnONPs creates both types of bacteria that are beneficial to its antibacterial action (Amjadi et al., 2019). The casting thickness was found to increase the G.CHNF.ZnONP film's antibacterial activity. The increase in the availability of ROS, which results from the reaction of Zn^{2+} with oxygen, as the film thickness increases, accelerates the death of bacterial cells (Kumar et al., 2020). The increase in thickness also causes an increase in porosity which intensifies the increased intracellular component leakage, resulting in cell death (Kravanja et al., 2019).

Table 1. Film color properties with the variation in composition

Sample	Parameter of Film's Color Properties					
	L*	a*	b*	YI	WI	ΔE
G	101.25	0.38	-0.41	0.54	99.06	9.31
G.CHNF	101.04	0.26	-0.34	0.37	99.37	8.34
G.ZnONPs	99.47	0.18	-0.01	0.26	99.84	3.64
G.CHNF.ZnONPs	97.08	0.02	0.70	0.03	95.49	1.15

ΔE: total color difference, WI: whiteness indices, and YI: yellowness indices
Data were expressed as mean ±47.05 standard deviation

Table 2. Film color properties with variation of casting thickness

Sample	Casting Thickness (mm)	Parameter of Film's Color Properties					
		L*	a*	b*	YI	WI	ΔE
G. CHNF. ZnONPs	0.8	97.39	0.07	0.19	1.10	96.57	1.79
	1.0	97.26	0.05	0.21	0.07	96.22	1.80
	1.2	97.17	0.03	0.7	0.04	95.75	1.10
	1.4	97.08	0.02	0.7	0.03	95.49	1.15

Data were expressed as mean ±46.26 standard deviation

Table 3. Inhibition zone of the edible packaging components against bacteria

Component	Inhibition Zone (mm)		
	Staphylococcus aureus	*Escherichia coli*	*Pseudomonas aeruginosa*
CHNF	15.50	18.06	16.53
ZnONPs	19.43	17.20	16.30

Data were expressed as mean ± 1.40 standard deviation (n=3)

Table 4. Antibacterial activity with a variation in composition

Sample	Inhibition Zone (mm)								
	Staphylococcus aureus			*Escherichia coli*			*Pseudomonas aeruginosa*		
	IZ (mm)	K (-) (mm)	K (+) (mm)	IZ (mm)	K (-) (mm)	K (+) (mm)	IZ (mm)	K (-) (mm)	K (+) (mm)
G	-			-			-		
G.CHNF	9.18	11.49	13.70	11.68	9.80	11.07	10.19	8.59	9.58
G.ZnONPs	12.65			11.38			10.03		
G.CHNF.ZnONP	14.63			12.30			11.15		

Data were expressed as mean ±1.68 standard deviation (n=3)

Table 5. Antibacterial activity of G.CHNF.ZnONP film with variations in cast thickness

Casting Thickness (mm)	Inhibition Zone (mm)								
	Staphylococcus aureus			*Escherichia coli*			*Pseudomonas aeruginosa*		
	IZ (mm)	K (-) (mm)	K (+) (mm)	IZ (mm)	K (-) (mm)	K (+) (mm)	IZ (mm)	K (-) (mm)	K (+) (mm)
0.8	11.15			9.66			8.38		
1.0	12.28	11.49	13.70	10.51	9.80	11.07	9.29	8.59	9.58
1.2	13.34			10.99			9.60		
1.4	14.63			12.30			11.15		

Data were expressed as mean ±1.78 standard deviation (n=3)

CONCLUSIONS

Gelatin-based nanocomposites containing CHNF and ZnONP have been prepared and characterized. Changes in the morphology of the G film were detected on SEM images with the addition of CHNF and ZnONP. Chitosan nanofibers create interconnected pore structures, while the presence of ZnONP suppresses the volume of free space in the gelatin matrix. As a result, the gelatin matrix's increase in density and compactness and the formation of a less permeable structure resulted in a G/CHNF/ZnONP film with the best mechanical and barrier properties. G/CHNF/ZnONP nanocomposites were also found to have the highest antibacterial activity compared to other films. In addition, the farthest shift was from the two endothermic peaks of the G.CHNF.ZnONP film, indicating a synergistic effect of CHNF, ZnONPs, and gelatin that increased the order of the gelatin chains. and film crystallinity. The film becomes more resistant to heat when the casting thickness is increased. The combination of CHNF and ZnONP had a synergistic impact, resulting in the greatest decrease in G.CNF transparency. This special characteristic enables G/CHNF/ZnONP films to enhance food freshness and prolong storage time, making them potential for packaging applications that require improved food quality and extended shelf life.

ACKNOWLEDGMENTS

The author is grateful to the Ministry of Education, Culture, Research, and Technology of the Indonesian Republic for funding this work through the Applied Research Grant program.

REFERENCES

Al-Tayyar, N. A., Youssef, A. M., & Al-Hindi, R. R. (2020). Antimicrobial packaging efficiency of ZnO-SiO_2 nanocomposites infused into PVA/CS film for enhancing the shelf life of food products. *Food Packaging and Shelf Life, 25*. doi:https://doi.org/10.1016/j.fpsl.2020.100523

Amjadi, S., Emaminia, S., Davudian, S. H., Pourmohammad, S., Hamishehkar, H., & Roufegarinejad, L. (2019). Preparation and characterization of gelatin-based nanocomposite containing chitosan nanofiber and ZnO nanoparticles. *Carbohydrate Polymers, 216*, 376-384. doi:https://doi.org/10.1016/j.carbpol.2019.03.062

Amjadi, S., Hamishehkar, H., & Ghorbani, M. (2019). A novel smart PEGylated gelatin nanoparticle for co-delivery of doxorubicin and betanin: A strategy for enhancing the therapeutic efficacy of chemotherapy. *Materials Science and*

Engineering: C, 97, 833-841. doi:https://doi.org/10.1016/j.msec.2018.12.104

ASTM. (2005). Morphological, physical, antimicrobial and release properties of ZnO nanoparticles-loaded bacterial 700 cellulose films. In *Annual book of ASTM*. Philadelphia: American Society for Testing and Materials.

Babaei-Ghazvini, A., Acharya, B., & Korber, D. R. (2021). Antimicrobial biodegradable food packaging based on chitosan and metal/metal-oxide bio-nanocomposites: A Review. *Polymers, 13*(16), 2790. doi:https://doi.org/10.3390/polym13162790

Bahar, A., Kusumawati, N., & Muslim, S. (2020). Preparation and characterization of goatskin gelatin as halal alternative to bovine gelatin. *Rasayan Journal of Chemistry, 13*(1), 85-98. doi:http://dx.doi.org/10.31788/RJC.2019.1245409

Bahar, A., Rusijono, & Kusumawati, N. (2018). Extraction and characterization of the base halal gelatin on bovine bone. *Advances in Engineering Research,* 171. doi:https://doi.org/10.2991/snk-18.2018.10

Bahar, A., Rusijono, R., & Kusumawati, N. (2019). The Effect of curing and extraction time against yield and quality of type b gelatin from goat bone. *Atlantis Highlights in Chemistry and Pharmaceutical Sciences, 1*, 5-9. doi:https://doi.org/10.2991/snk-19.2019.2

Boura-Theodoridou, O., Giannakas, A., Katapodis, P., Stamatis, H., Ladavos, A., & Barkoula, N.-M. (2020). Performance of ZnO/chitosan nanocomposite films for antimicrobial packaging applications as a function of NaOH treatment and glycerol/PVOH blending. *Food Packaging and Shelf Life, 23*. doi:https://doi.org/10.1016/j.fpsl.2019.100456

Cai, L., Shi, H., Cao, A., & Jia, J. (2019). Characterization of gelatin/chitosan polymer films integrated with docosahexaenoic acids fabricated by different methods. *Scientific Reports, 9*. doi:https://doi.org/10.1038/s41598-019-44807-x

Cai, J., Xiao, J., Chen, X., & Liu, H. (2020). Essential oil loaded edible films prepared by continuous casting method: Effects of casting cycle and loading position on the release properties. *Food Packaging and Shelf Life*, *26*(August), 100555. https://doi.org/10.1016/j.fpsl.2020.100555

Chen, C., Deng, S., Yang, Y., Yang, D., Ye, T., & Li, D. (2018). Highly transparent chitin nanofiber/gelatin nanocomposite with enhanced mechanical properties. *Cellulose, 25*, 5063-5070. doi:https://doi.org/10.1007/s10570-018-1915-z

Chen, C., Wang, Y., Yang, Y., Pan, M., Ye, T., & Li, D. (2018). High strength gelatin-based nanocomposites reinforced by surface-deacetylated chitin nanofiber networks. *Carbohydrate Polymers, 195*, 387-392. doi:10.1016/j.carbpol.2018.04.095

Davoodi, S., Davachi, S. M., Golkhajeh, A. G., Shekarabi, A. S., & Abbaspourrad, A. (2020). Development and characterization of Salvia macrosiphon/chitosan edible films. *ACS: Sustainable Chemistry and Engineering, 8*(3), 1487-1496. doi:https://doi.org/10.1021/ascsuschemeng.9b05894

Ebrahimi, S., Fathi, M., & Kadivar, M. (2019). Production and characterization of chitosan-gelatin nanofibers by nozzle-less electrospinning and their application to enhance edible film's properties. *Food Packaging and Shelf Life, 22*. doi:https://doi.org.10.1016/j.fpsl.2019.100387

Ge, S., Liu, Q., Li, M., Liu, J., Lu, H., Li, F., . . . Xiong, L. (2018). Enhanced mechanical properties and gelling ability of gelatin hydrogels reinforced with chitin whiskers. *Food Hydrocolloids, 75*, 1-12. doi:https://doi.org/10.1016/j.foodhyd.2017.09.023

Hari, K. D., Garcia, C. V., Shin, G.-H., & Kim, J.-T. (2021). Improvement of the UV barrier and antibacterial properties of crosslinked pectin/zinc oxide bionanocomposite films. *Polymers, 13*(15). doi:https://doi.org/10.3390/polym13152403

Kamdem, D. P., Shen, Z., Nabinejad, O., & Shu, Z. (2019). Development of biodegradable composite chitosan-based films incorporated with xylan and carvacrol for food packaging application. *Food Packaging and Shelf Life, 21*. doi:https://doi.org/10.1016/j.fpsl.2019.100344

Kan, J., Liu, J., Yong, H., Liu, Y., Qin, Y., & Liu, J. (2019). Development of active packaging based on chitosan-gelatin blend films functionalized with Chinese hawthorn (Crataegus pinnatifida) fruit extract. *International Journal of Biological Macromolecules, 140*, 384-392. doi:10.1016/j.ijbiomac.2019.08.155

Kravanja, G., Primozic, M., Knez, Z., & Leitgeb, M. (2019). Chitosan-based (nano)materials for novel biomedical applications. *Molecules, 24*(10), 1960. doi:10.3390/molecules24101960

Kumar, S., Mudai, A., Roy, B., Basumatary, I. B., Mukherjee, A., & Dutta, J. (2020). Biodegradable hybrid nanocomposite of chitosan/gelatin and green synthesized zinc oxide nanoparticles for food packaging. *Foods, 9*(9), 1143. doi:https://doi.org/10.3390/foods9091143

Kusumawati, N., Bahar, A., Maria, M. S., & Muslim, S. (2019). Impact of curing and extraction time on yield and quality of base gelatin from goat skin. *IOP Conference Series: Earth and Environmental Science, 347*. doi:10.1088/1755-1315/347/1/012083

Li, Y., Yang, G., Deng, D., & Zhang, Y. (2021). Effect of chromium coating thickness on surface adhesion of polyethylene terephthalate optical film. *Surfaces and Interfaces*, *26*(August), 101429. https://doi.org/10.1016/j.surfin.2021.101429

Lin, L., Gu, Y., & Cui, H. (2019). Moringa oil nanoparticles embedded gelatin nanofibers for food packaging against Listeria monocytogenes and *Staphylococcus aureus* on cheese. *Food Packaging and Shelf Life, 19*, 89-93. doi:https://doi.org/10.1016/j.fpsl.2018.12.005

Liu, C., Huang, J., Zheng, X., Liu, S., Lu, K., Tang, K., & Liu, J. (2020). Heat sealable soluble soybean polysaccharide/gelatin blend edible films for food packaging applications. *Food Packaging and Shelf Life, 24*. doi:https://doi.org/10.1016/j.fpsl.2020.100485

Nandiwilastio, N., Muchtadi, T. R., Suyatma, N. E., & Yuliani, S. (2019). Effect of the addition of beeswax and zinc oxide nanoparticles on the physical and mechanical properties of chitosan-based films *Jurnal Teknologi dan Industri Pangan, 30*(2), 119-126. doi:https://doi.org/10.6066/jtip.2019.30.2.119

Ngo, T. M., Dang, T. M., Tran, T. X., & Rachtanapun, P. (2018). Effects of zinc oxide nanoparticles on the properties of pectin/alginate edible films. *International Journal of Polymer Science,* 2018. doi:https://doi.org/10.1155/2018/5645797

Quero, F., Padila, C., Campos, V., Luengo, J., Caballero, L., Melo, F., . . . Enrione, J. (2018). Stress transfer and matrix-cohesive fracture mechanism in microfibrillated cellulose-gelatin nanocomposite films. *Carbohydrate Polymers, 195*, 89-98. doi:https://doi.org/10.1016/j.carbpol.2018.04.059

Roy, S., & Rhim, J.-W. (2021). Fabrication of bioactive binary composite film based on gelatin/chitosan incorporated with cinnamon essential oil and rutin. *Colloids and Surfaces B: Biointerfaces, 204*. doi:https://doi.org/10.1016/j.colsurfb.2021.111830

Rudakova, A. V., Emeline, A. V., Romanychev, A. I., & Bahnemann, D. W. (2021). Photoinduced hydrophilic behavior of TiO2 thin film on Si substrate. *Journal of Alloys and Compounds*, *872*, 159746. https://doi.org/10.1016/j.jallcom.2021.159746

Shankar, S., Wang, L.-F., & Rhim, J.-W. (2017). Preparation and properties of carbohydrate-based composite films incorporated with CuO nanoparticles. *Carbohydrate Polymers, 169*, 264-271. doi:https://doi.org/10.1016/j.carbpol.2017.04.025

Soradech, S., Nunthanid, J., Limmatvapirat, S., & Luangtana-anan, M. (2017). Utilization of shellac and gelatin composite film for coating to extend the shelf life of banana. *Food Control, 73*, 1310-1317. doi:https://doi.org/10.1016/j.foodcont.2016.10.059

Susmitha, A., Sasikumar, K., Rajan, D., Padmakumar M, A., & Nampoothiri, K. M. (2021). Development and characterization of corn starch-gelatin based edible films incorporated with mango and pineapple for active packaging. *Food Bioscience, 41*. doi:https://doi.org/10.1016/j.fbio.2021.100977

Wafi, A., Atmaja, L., & Ni'mah, Y. L. (2020). Analysis of tensile strength and elongation of the gelatin-chitosan film. *Alchemy Journal of Chemistry, 8*(1). doi:https://doi.org/10.18860/al.v8i1.9097

Wang, H., Ding, F., Ma, L., & Zhang, Y. (2021). Edible films from chitosan-gelatin: physical properties and food packaging application. *Food Bioscience, 40*. doi:https://doi.org/10.1016/j.fbio.2020.100871

Yadav, S., Mehrotra, G. K., & Dutta, P. K. (2021). Chitosan based ZnO nanoparticles loaded gallic-acid films for active food packaging. *Food Chemistry,* 334. doi:https://doi.org/10.1016/j.foodchem.2020.127605

Yusof, N. A., & Zain, N. M. (2019). The effect of ZnO nanoparticles on the physical, mechanical, and antibacterial properties of chitosan-gelatin hydrogel films. *Jurnal Teknologi, 81*(2). doi:https://doi.org/10.11113/jt.v81.12605

Zhang, H., & Wang, W. (2017). Mold simulator study of heat transfer phenomenon during the initial solidification in continuous casting mold. *Metallurgical and Materials Transactions*, *48*, 779–793.